AN INVESTIGATION OF THE FLEXURAL VIBRATION BEHAVIOR OF SLENDER ROTORS IN DRUM-TYPE CONDENSING TURBINES

by

Rolf Sparmann

Head, Development Section

Industrial Turbine Division

Siemens AG

Wesel, West Germany

Rolf Sparmann, Dipl.-Ing. is the head of the Development Section of the Siemens turbine works in Wesel (in the Federal Republic of Germany). He is in charge of the design of industrial turbines under development and of the turbine calculation procedures. Mr. Sparmann has worked in the field of large power station steam turbines, turbocompressors and industrial steam turbines for more than 15 years. He graduated from the Technical University in Hannover.

ABSTRACT

With turbine rotors of low shaft elasticity (large diameter and small bearing span) the increase in amplitude at the first point of shaft resonance in the speed range is generally slight. Consequently no particular attention is paid to this point of resonance either at the rotor design stage or during operation of the turbine.

However, if a two-cylinder condensing turbine has to be replaced by a single-cylinder machine of similar high efficiency, it is necessary to have a drum-type rotor of large bearing span and small diameter in the region of the first drum stages, and large diameter in the region of the low-pressure stages.

This type of rotor has a markedly higher shaft elasticity compared with the rotors of the two-cylinder machine.

A rotor of this type was recently built and put into service. This paper describes the rotor and gives its calculated dynamic characteristics. Since operation in the vicinity of the first resonant speed is of greatest interest the paper describes the test results for the properly balanced condition, and for the artificially heavily unbalanced condition.

The shaft vibration values measured during the test-run are compared with the assessment criteria for rotor dynamic performance used at present.

In order to obtain valid theoretical statements for even more slender rotors, the shaft elasticity was systematically increased in theoretical calculations (by increasing the bearing span). The effects of the shaft elasticity on the magnitude of the resonant speeds, the maximum vibration amplitudes and the stability limit (oil whip) are described.

In its original form, the drum-type rotor studied here has only one output shaft coupling. For even higher turbine powers, however, heavy couplings on both shaft ends are necessary.

In order to examine the dynamic behavior of these rotors, the original rotor was fitted with an extra mass at the usually free shaft-end to simulate a second coupling. For this rotor, the same calculations and measurements were carried out in the overspeed testing pit as were for the original rotor. The results are given and discussed. A further point examined with this rotor is whether there is a linear relationship between the dynamic bearing force and the magnitude of the unbalance.

INTRODUCTION

Since it is almost impossible to undertake any subsequent correction of possible unsatisfactory performance of a finished rotor, it is necessary to be able to calculate the dynamic behavior of steam turbine rotors accurately at the preliminary design stage.

Modern calculation methods of rotor dynamics allow for the exact geometry of the rotor (mass distribution, pattern of moments of intertia), the modulus of elasticity of the material as a function of rotor temperature, the spring and damping properties of the oil film between the rotor and the journal bearing shells, and the spring constants of the bearing housings themselves.

The spring and damping properties of the oil film in the journal bearing are replaced by four spring constants and four damping constants per bearing for the purpose of calculation as seen in Figure 1.

In addition to the principal spring constants γ_{11} γ_{22} and the principal damping constants β_{11} and β_{22} there are also the respective linking terms γ_{12}, γ_{21} and β_{12}, β_{21}. The linking terms are explained as follows: If a force acts in the y direction (see Figure 1) on a shaft rotating in a journal bearing, the shaft reacts not only with a deflection in the direction of the force, but also in a positive or negative x direction depending on the direction of rotation. Mathematically speaking, these values are the linking terms between the equations of motion of the rotor in the x and y directions.

The dynamic bearing forces F_x and F_y result as reaction to the displacements x and y and the displacement velocities $\dot{x}$ and $\dot{y}$:

$$F_x = \gamma_{11} \cdot x + \gamma_{12} \cdot y + \beta_{11} \cdot \dot{x} + \beta_{12} \cdot \dot{y} \qquad (1)$$

$$F_y = \gamma_{21} \cdot x + \gamma_{22} \cdot y + \beta_{21} \cdot \dot{x} + \beta_{22} \cdot \dot{y} \qquad (2)$$

Experimental determination of the spring and damping constants giving good agreement with theoretical values has been performed by Glienecke [1].

Pollmann [2] [3] improved the agreement between experiment and theory by taking into account the change in oil viscosity across the lubricating gap in circumferential direction. Thus, today it is possible to calculate the spring and damping constants with adequate accuracy for any journal bearing geometry [4]. Details of the methods employed for calculating rotor dynamic performance are given in references [5] and [6].
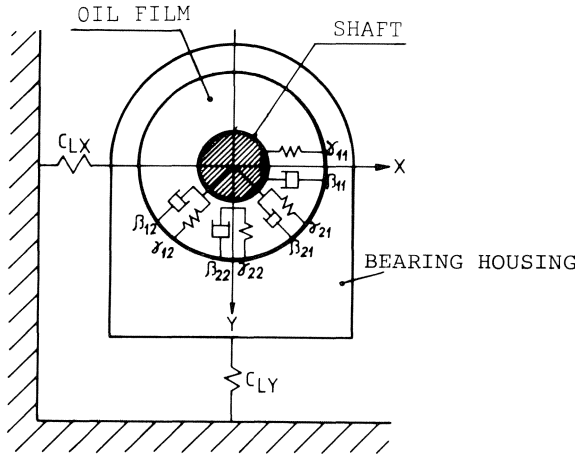
γ — SPRING CONSTANT OF OIL FILM

β — DAMPING CONSTANT OF OIL FILM

c_L — SPRING CONSTANT OF B-HOUSING

$\gamma_{11}, \gamma_{22}, \beta_{11}, \beta_{22}$ — PRINCIPAL SPRING AND DAMPING CONSTANTS

$\gamma_{12}, \gamma_{21}, \beta_{12}, \beta_{21}$ — LINK TERM SPRING AND DAMPING CONSTANTS

Figure 1. Diagram of Spring and Damping Constants of the Oil Film and the Spring Constants of the Bearing Housing.

SIMILARITY VALUES FOR ROTOR DYNAMICS

If the same dynamic behavior is expected of two rotors, journal bearings with the same clearance geometry for the supporting oil film and the same length/diameter ratio must be used. It is equally important, however, that the dynamic similarity values are also identical: the displacement of the shaft in the oil film and the magnitude of the spring and damping constants are determined by the Sommerfeld number S_o and the similarity number for temperature rise K_t according to Pollmann [2], which takes into account the varying viscosity in the oil film.

$$S_o = \frac{F_{stat} \cdot \psi^2}{B \cdot D \cdot \eta_E \cdot \omega} \qquad (3)$$

$$K_t = \frac{\eta_E \cdot \omega}{c \cdot \rho \cdot \vartheta_E \cdot \psi^2} \qquad (4)$$

F_{Stat} = Static bearing force

ψ = Relative minimum bearing clearance

B = Supporting bearing length

D = Bearing journal diameter

η_E = Oil viscosity at reference temperature ϑ_E

ω = Angular velocity of rotor

c = Specific heat of oil

ρ = Specific gravity of oil

The shaft-bearing system is identified by the shaft elasticity μ:

$$\mu = f / \Delta R \qquad (5)$$

ΔR = Minimum radial bearing clearance

$$\Delta R = D \cdot \psi / 2 \qquad (6)$$

f = Sag due to weight of a massless shaft having the mass of the rotor concentrated as a point mass at the center. f is made so that this single-mass vibration system has the same first critical angular velocity ω_{KL}^* for rigid bearing support as the turbine rotor in question.

Therefore $\omega_{K1}^* = \sqrt{c/m} \qquad (7)$

$c = m \cdot g/f \qquad (8)$

$\mu = f/\Delta R = g/\Delta R \cdot \omega_{K1}^{*2} \qquad (9)$

g = Acceleration due to gravity

So that two rotors can be compared dynamically, S_o and K_T are obtained for the first critical speed ω_{K1}^* of the rigidly supported rotor:

$$S_{oK} = \frac{F_{stat} \cdot \psi^2}{B \cdot D \cdot \omega_{K1}^*} \qquad (10)$$

$$K_{TK} = \frac{\eta_E \cdot \omega_{K1}^*}{c \cdot \rho \cdot \vartheta_E \cdot \psi^2} \qquad (11)$$

If the rotors being compared have similar journal bearings and similar values S_{oK}, K_{TK} and μ, their dynamic behavior will be largely identical at least up to the first rotor resonant speed.

ROTOR FOR A CONDENSING TURBINE WITH *ONE* COUPLING

The rotor being studied is shown in Figure 2 which gives all principal data. Figure 3 shows the sections into which the rotor is divided for calculating the dynamic behavior and also the temperature variation for the modulus of elasticity of the material.

In Figures 4, 5 and 6, the calculated amplitude values of rotor vibration are plotted as a function of speed. The amplitude values A are defined as half the major axis of the ellipse of motion of the rotor center. The amplitude values are plotted for the front free shaft end (o), the two bearing journals (2) and (6), midway between the bearing span (4) and the rear shaft end carrying the coupling (8).

Figure 4, 5 and 6 differ in the unbalance arrangement chosen. Basically, the actual distribution of the unbalance of a turbine rotor is unknown. During balancing, it is only possible to measure the resulting unbalance vectors at the bearings. To assess the dynamic behavior of the rotor, therefore, it is necessary to make assumptions about the unbalance. They are chosen so that, if possible, all natural frequencies of the rotor are thoroughly excited.

So that different rotors can be compared with each other, the same balance assumptions for the calculation are always used. The assumption itself comprises the position and magnitude of the unbalance and, when there are several, also the phase position and the ratio of the magnitudes of the individual unbalances.

Figure 4 is applicable to an unbalance at mid bearing span, Figure 5 for two opposite-phase points of unbalance within the bearing span and Figure 6 corresponds to Figure 5 but with an additional opposite-phase unbalance at the two shaft ends.

Since a linear equation system is used for calculating the shaft vibration amplitude values A, the amplitude A is directly proportional to the chosen unbalance value U: twice the value
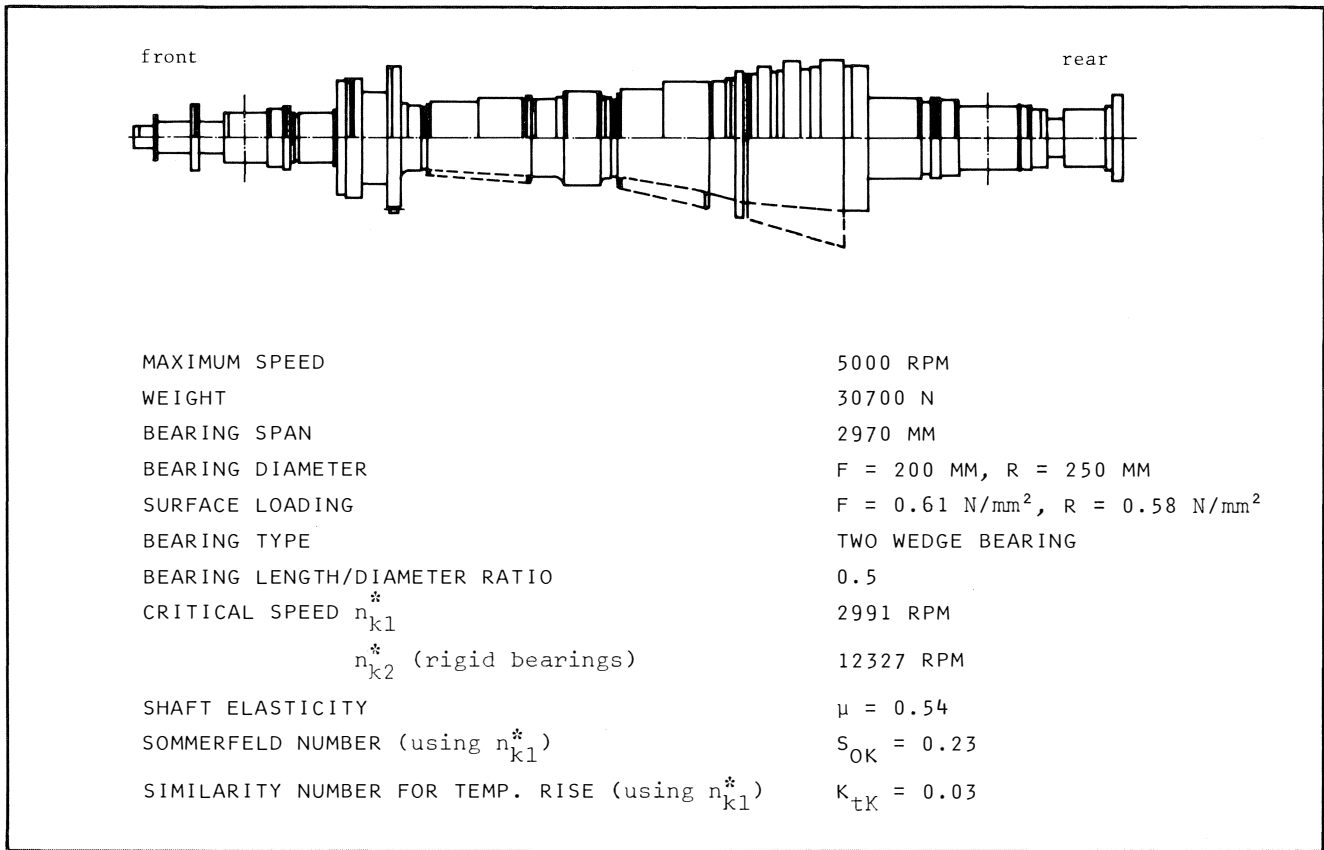
front   rear

MAXIMUM SPEED	5000 RPM
WEIGHT	30700 N
BEARING SPAN	2970 MM
BEARING DIAMETER	F = 200 MM, R = 250 MM
SURFACE LOADING	F = 0.61 N/mm^2, R = 0.58 N/mm^2
BEARING TYPE	TWO WEDGE BEARING
BEARING LENGTH/DIAMETER RATIO	0.5
CRITICAL SPEED n_{k1}^*	2991 RPM
n_{k2}^* (rigid bearings)	12327 RPM
SHAFT ELASTICITY	μ = 0.54
SOMMERFELD NUMBER (using n_{k1}^*)	S_{OK} = 0.23
SIMILARITY NUMBER FOR TEMP. RISE (using n_{k1}^*)	K_{tK} = 0.03

Figure 2. Condensing Turbine Rotor Studied With Principal Data.

(°C)   TEMPERATURE PATTERN

Rotor radius in mm

Mass diameter   Moment of inertia
                                   diameter

Bearing 1   ⓪ - ⑧ = Identification of locations of rotor vibration   Bearing 2
                            amplitudes as shown in Figs. 4 - 8
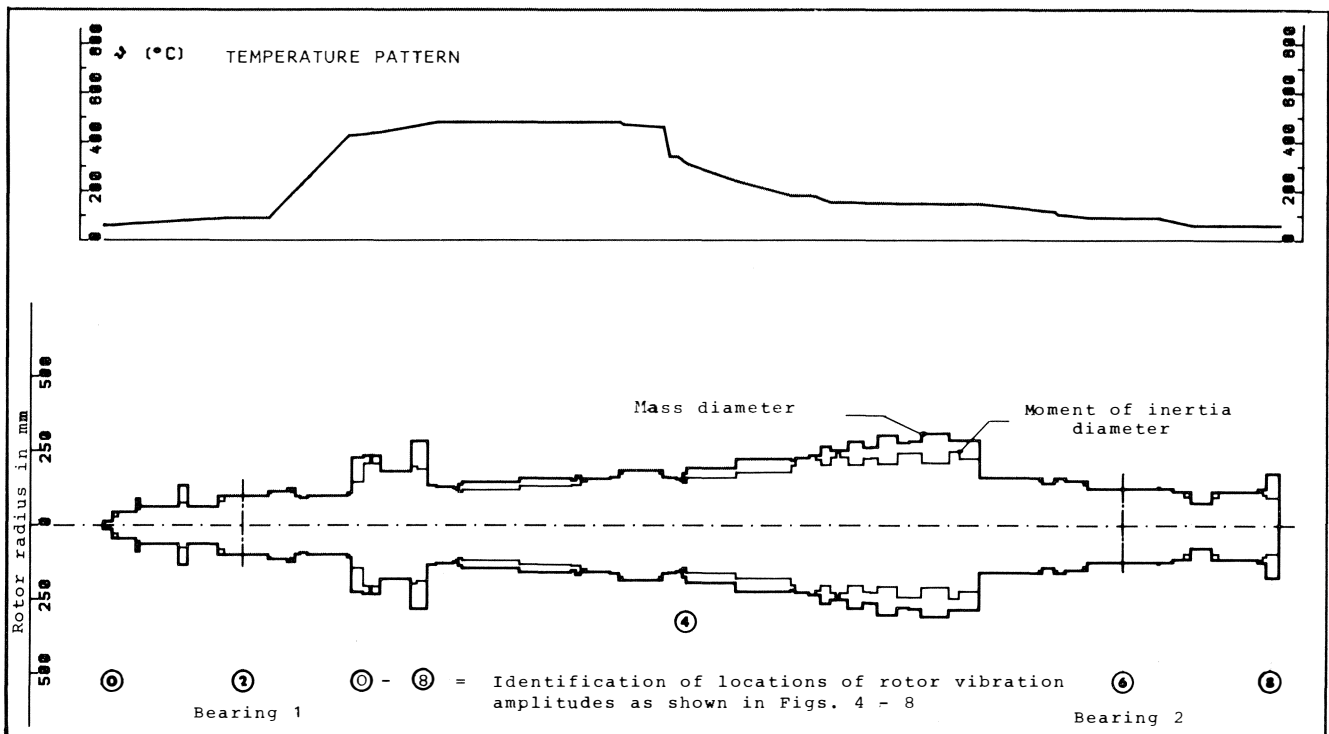
Figure 3. Rotor, Divided into Sections; Rotor Temperature Pattern, and Locations of Points, Used for the Calculation of Vibration Amplitudes.
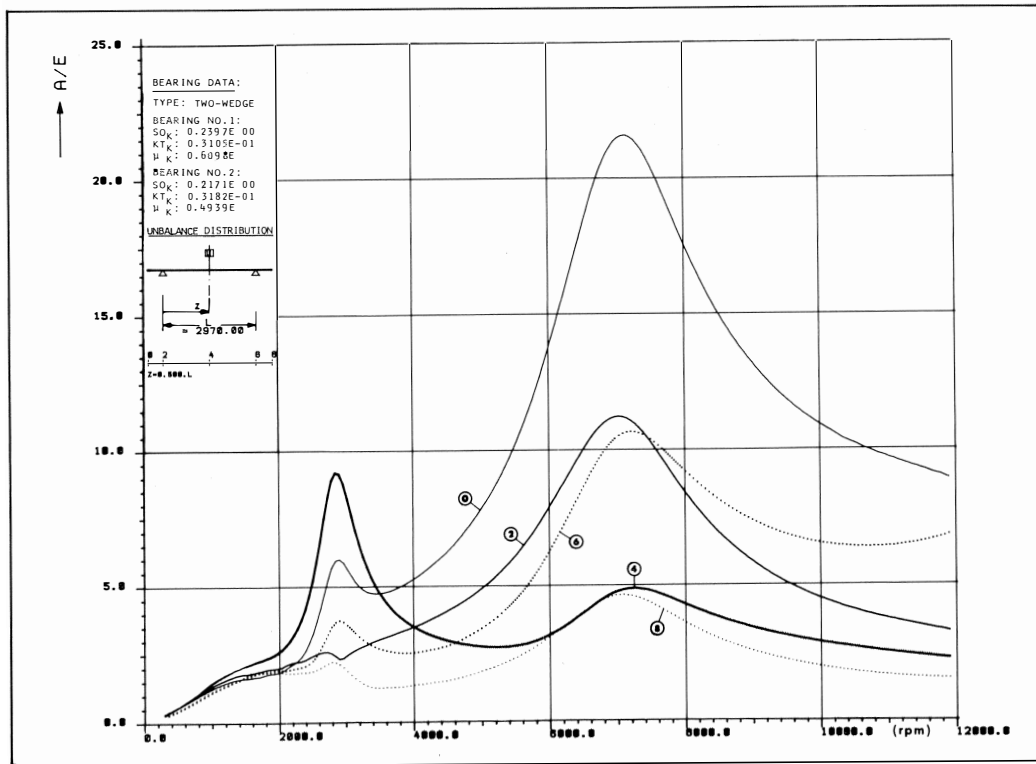
Figure 4. *Relative Amplitudes of Shaft Vibration as a Function of Speed for One Unbalance in the Center of the Rotor. (Rotor as in Figure 2, Location of Calculation Points as per Figure 3).*
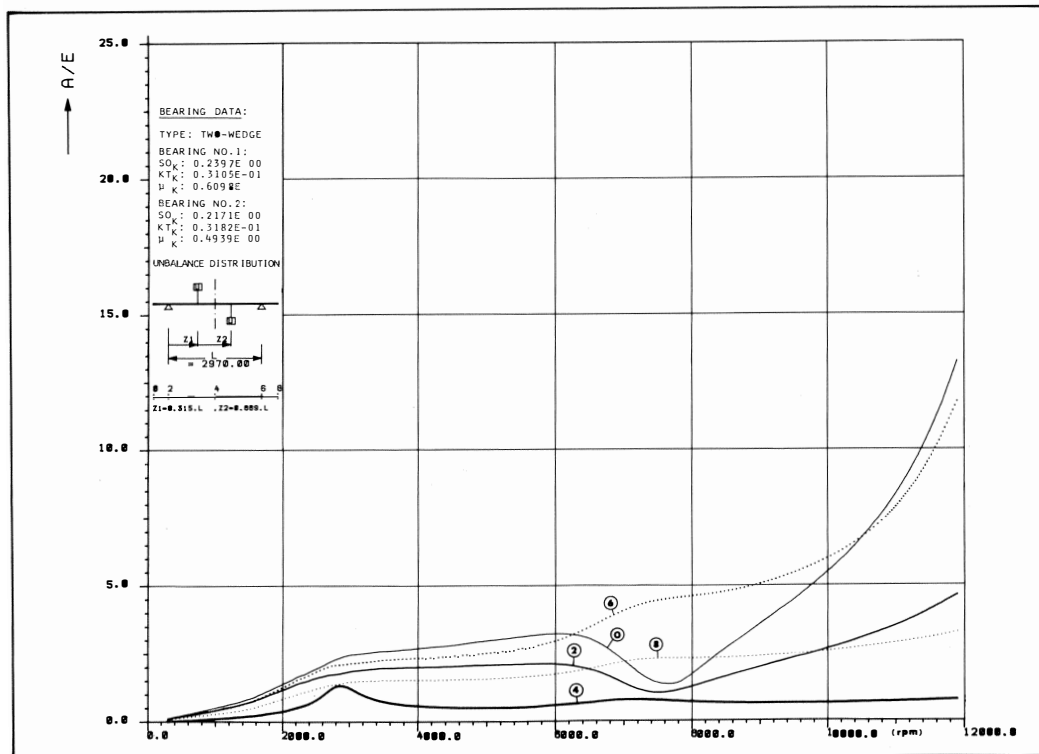
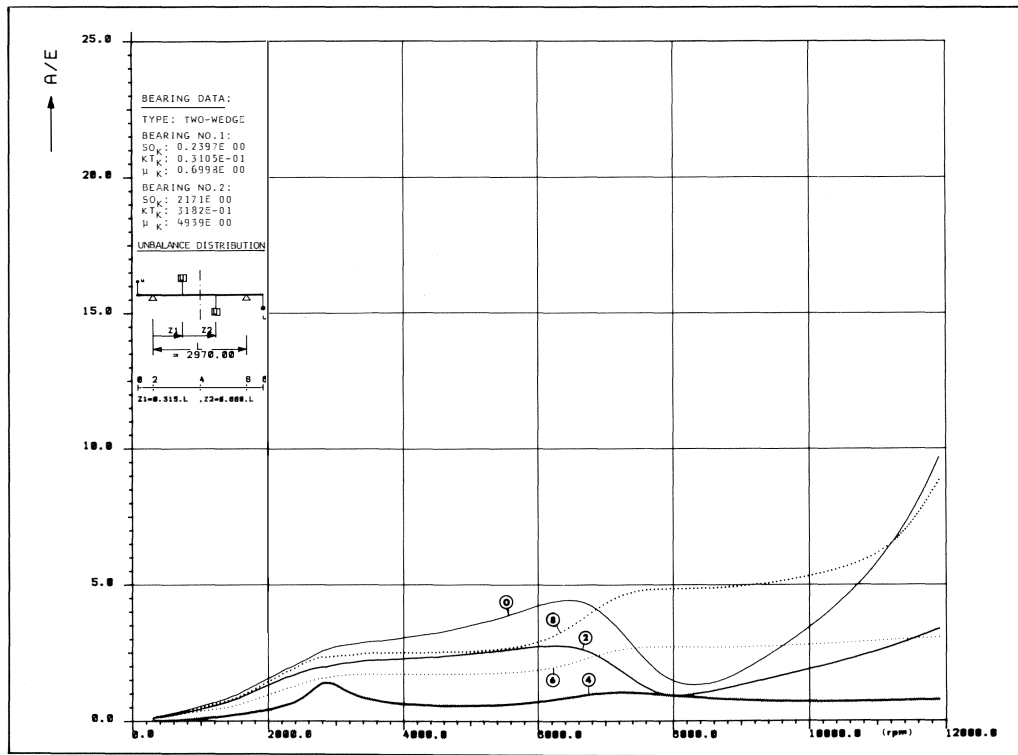Figure 5. *As Figure 4, but with Two Unbalance Points Opposite in Phase*

Figure 6. As Figure 4, but with Four Unbalance Points Opposite in Phase.

U gives twice the value A so the quotient A/U remains constant. The unbalance radius e is introduced in place of the unbalance U:

$$e = \frac{U}{m_{rotor}} \tag{12}$$

m_{rotor} = Total mass of rotor

The unbalance U then has the dimensions length x mass. The shaft vibration amplitude values are plotted in Figures 4, 5 and 6 as relative values A/e. The unbalance itself must be chosen large enough so that the calculation is numerically stable. The choice of magnitude has no effect on the result of the calculation. If several points of unbalance are used, the unbalance radius e is defined as follows:

$$e = \frac{\sum U}{m_{rotor}}$$

$\sum U$ = Sum of all unbalance values.

The assumption that A/e is independent of the magnitude of the unbalance assumed is only applicable now provided the ratio of the magnitudes of the unbalances to each other is not changed.

From Figures 4, 5 and 6 it can be seen that the first and second points of rotor resonance are excited most strongly by the center unbalance. The first point of resonance is at n_{k1} = 2872 rev/min, the second at n_{k2} = 7154 rev/min. At n_{k1} the rotor center exhibits maximum deflection whereas at n_{k2} it is the front shaft end. Since the relative values A/e have no relation to the values which must be attained during the acceptance testing of turbines, the relevant amplitude values A have been calculated for an attainable balance grade of the

rotor assuming center unbalance. These amplitude values are compared with the maximum values to API 612 [8].

Balance grade is defined by VDI 2060 [9] as:

$$Q = e \cdot \omega \tag{13}$$

$$e = Q / \omega \tag{14}$$

Q = Balance grade expressed as vibration velocity
ω = Angular velocity of rotor

Thus, a requirement for constant balance grade Q necessitates ever smaller radii e for the residual unbalance of the rotor with increasing speed.

The values (A/e) are obtained from the vibration calculation:

$$A = (A/e) \cdot e = (A/e) \cdot Q/\omega \tag{15}$$

To calculate the amplitude A it is necessary to have a value for the unbalance radius e. This can be calculated for an attainable balance grade Q and a selected balance speed with equation (14). If the balance speed is taken as the maximum operating speed, the balance grade Q from equation (13) becomes proportionally better for all low speeds.

In order to be able to make the most unfavorable assumption for the magntiude of the unbalance radius for the whole speed range, e is varied, but Q is held constant. In consequence, e becomes a function of the speed.

This assumption has the advantage that every speed can also be the balance speed.

For comparing the amplitude A with the acceptance limits to API, the balance grade Q is taken as unity.

Hence, $e = 1/\omega$ $\tag{16}$

In Figure 7 the amplitude values for the bearing journals (positions 2 and 6 on the rotor) must be compared with the API values. The amplitude values for the assumed balance grade Q = 1 are considerably below the API values. The splitting of the first resonant speed, due to the two-wedge bearing, can be clearly seen in Figure 7: the resonant point below n_{k1} (defined by the maximum amplitude of the rotor center, i.e. position 4) also appears in Figure 4, but the unbalance is very small due to e being constant, and with the low value of ω, so that the amplitude remains small. In Figure 7, on the other hand, the unbalance radius assumes very large values at low speeds, thus producing large amplitudes because of the very large unbalance. The reverse applies to the higher speed range.

The API values are acceptance values for demonstrating good balancing of a machine. However, for turbine operation such amplitude values do not represent a danger limit.

In order to illustrate the difference between the API values and the "alarm limit", the alarm-limit values, according to the new VDI 2059 [10], have been entered in Figure 7. The alarm limit has been calculated for a rotor which, at commissioning, had shaft vibration values corresponding to API 612.

During test runs of the properly balanced rotor, the values of rotor amplitude shown in Figure 7 were measured at the bearings. The calculated values and measured values are only suitable for limited comparison because the unbalance distribution of the balanced rotor is unknown and certainly will not correspond to the calculation assumption of a single center unbalance.

There is good agreement between measurement and calculation for the position of the points of resonance. This proves the excellent accuracy of the oil film spring constants being used.

At the maximum balancing speed of n_{max} = 5000 rev/min there is also good agreement between calculation and measurement for the amplitude values. At higher speeds the measured curves rise more steeply than the calculated ones because here the actual balance grade is worse than Q = 1. At lower speeds, however, the calculated values rise more steeply because the actual rotor exhibits a balance grade better than Q = 1 at these speeds.

In order to examine the sensitivity of the rotor to coupling unbalance, a second absolute amplitude curve has been calculated for a single unbalance on the coupling. However, Q = 40 is used for the balance grade; although the coupling hub and sleeve are balanced to Q = 1 to Q = 2.5, respectively, the actual unbalance can become much greater due to the tooth clearance and as a result of wear.

The absolute amplitude values are not compared with API 612 in Figure 8, because it is an unusual disturbance condition which is being assessed.

The amplitudes at the bearings 2 and 6 are therefore compared with the "alarm limit" to VDI 2059. Even for this large coupling unbalance the vibration amplitude in the bearings only reaches approximately one quarter of the alarm limit values.

In Figures 9 to 12 the deflection curves of the rotor are shown in two planes for four different speeds: the lowest speed is below n_{k1}, the second is equal to n_{k1}, the third is between n_{k1} and n_{k2} and the fourth is equal to n_{k2}. Since the occurrence of major center unbalance due to rotor distortion or blade fracture is to be studied as a disturbance condition for this rotor, only a center unbalance is assumed.

For all speeds the deflection curve remains in the half-wave form. The shaft becomes increasingly deflected at the bearings with rising speed because of the spring properties of the oil film. The changeover from the half-wave to the full-wave curve, which takes place with rigid bearing support of the shaft when the second critical speed is approached, no longer occurs. For the first two speeds the maximum shaft deflection is found the middle of the rotor, whereas for the last two speeds it is at the front shaft end.

Dynamic bearing forces measured during balancing are plotted on a graph in Figure 13. The sum of the dynamic forces of both bearings has been referred to the rotor weight and is shown as a function of speed.

Curve 1 applies to the properly balanced rotor. At the maximum operating speed n_{max} = 5000 rev/min, the sum of the dynamic bearing forces is approximately 10% of the rotor weight and at the first resonant speed it is approximately 15%.

To examine the behavior of the rotor when passing through the first resonant speed for a disturbance condition of very large center unbalance, a single mass of 400 grams corresponding to an unbalance of 60×10^3 mmg was placed at mid bearing span. This unbalance corresponds to that of blade damage in which two moving blades have broken off completely in each of four rows in the center rotor area. The additional unbalance results in a balance grade of Q = 5.9 for the first resonant speed.

The sum of the measured dynamic bearing forces is shown as curve 2; at the first resonant speed it reaches 90% of the rotor weight. The factor of increase compared with the value for the properly balanced rotor is therefore approximately 6.

In the overspeed testing pit it was found possible to pass through the resonant speed without difficulty. This shows that it would be possible to safely shut down a turbine incorporating this slender drum-type rotor after the occurrence of major unbalance at operating speed.

THEORETICAL EXAMINATION OF THE EFFECT OF SHAFT ELASTICITY μ RESONANT SPEED AND AMPLITUDE

The shaft elasticity of the original rotor is approximately μ = 0.5. By increasing the bearing span, the μ value is increased in three steps to μ = 1. The rotor geometry used for the calculation is shown in Figure 14.

Figure 15 shows the effect of μ on the resonant speeds: with increasing shaft elasticity the resonant speeds fall, but from μ = 0.5 to μ = 1.0 the speed decrease $(n_{k2} - n_{k1})$ is only about 7%. Thus, the usable speed range between the two points of resonance is practically independent of the shaft elasticity. This is due to the oil film in the journal bearings, for with rigid bearings the speed range is reduced by 33%.

Figure 16 shows the ratio of the resonant speed n_k with the oil film effect to the resonant speed n_k^* for rigid bearings. The first resonant speed, n_{k1}/n_{k1}^* is almost independent of μ; whereas, for the second resonant speed, n_{k2}/n_{k2}^* rises sharply with increasing μ. This is the reason for the constant usable speed range mentioned in connection with Figure 15. It follows from Figure 16, generally, that with increasing shaft elasticity, the resonant speeds come closer and closer to those for rigid bearings.

In Figure 17 the effect of the shaft elasticity on the maximum rotor amplitude for the first resonant speed is shown. This maximum rotor amplitude has been calculated for position 4 (mid bearing span).

For a rotor supported in two-wedge bearings, a doubling of the shaft elasticity also doubles the resonant amplitude values. Thus, the disadvantage of high shaft elasticity is high resonant amplitude values when passing through the first re-
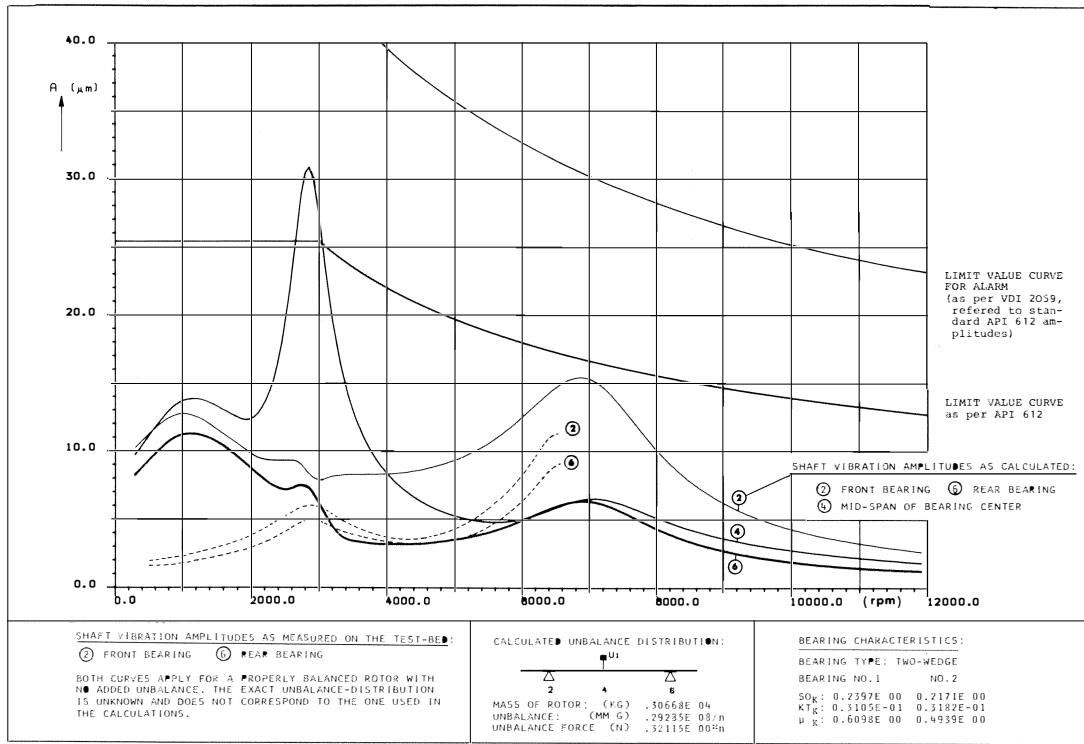
Figure 7. Amplitudes of Shaft Vibration for Unbalance Corresponding to Balance Grade Q = 1 of the Rotor as in Figure 2, Location of Calculation Points as per Figure 3.
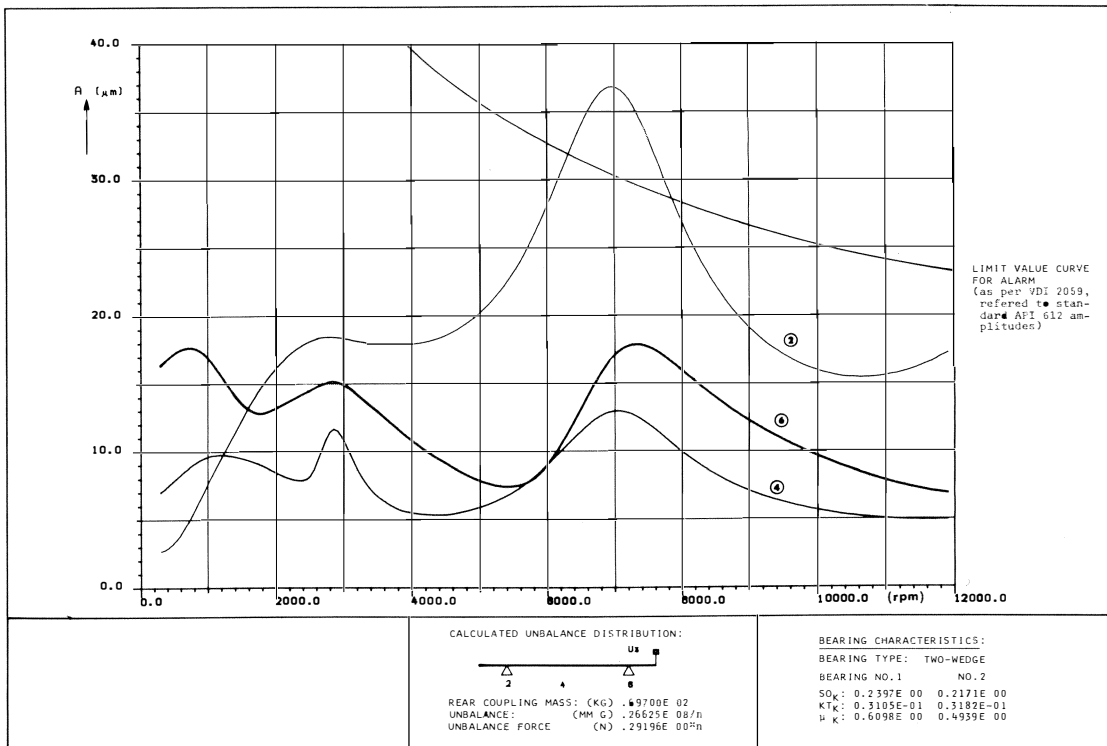
Figure 8. Amplitudes of the Shaft Vibration for an Unbalance at the Coupling Corresponding to Balance grade Q = 40 of the Coupling (Rotor as in Figure 2, Location of Calculation Points as per Figure 3).
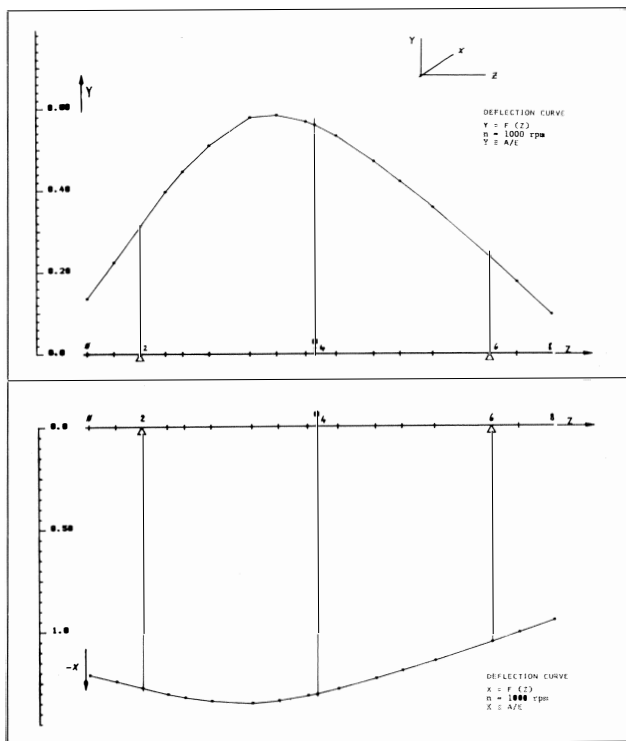
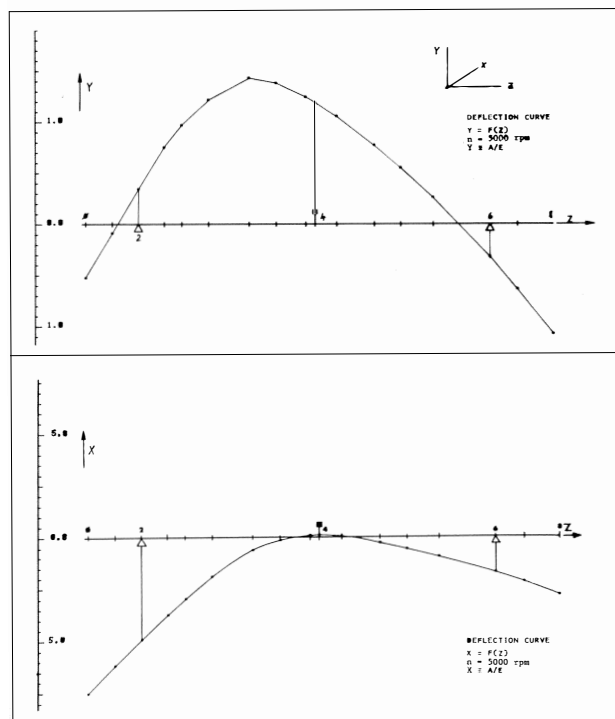Figure 9. *Deflection Curve for Unbalance at the Middle of the Rotor, n = 1000 rev/min (Rotor as in Figure 2).*

Figure 11. *As Figure 9, but n = 5000 rev/min.*
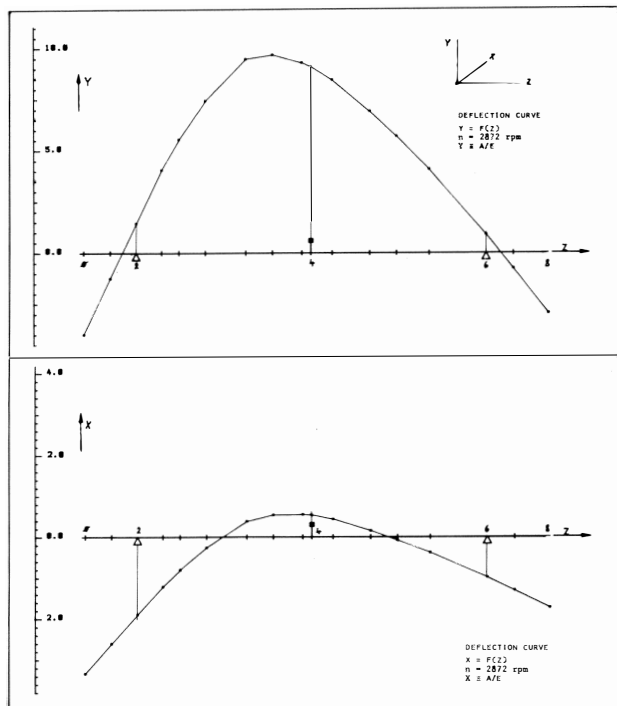
Figure 10. *As Figure 9, but n = 2872 rev/min.*
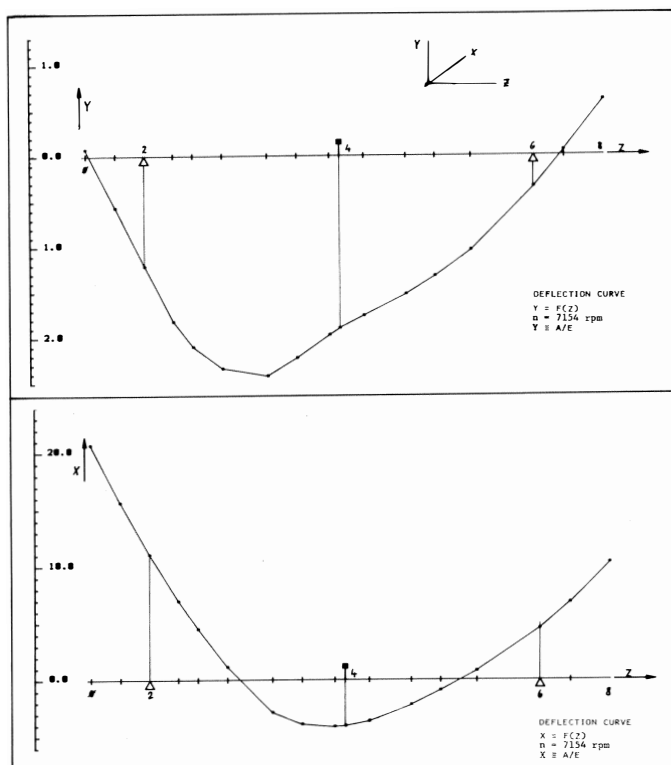
Figure 12. *As Figure 9, but n = 7154 rev/min.*
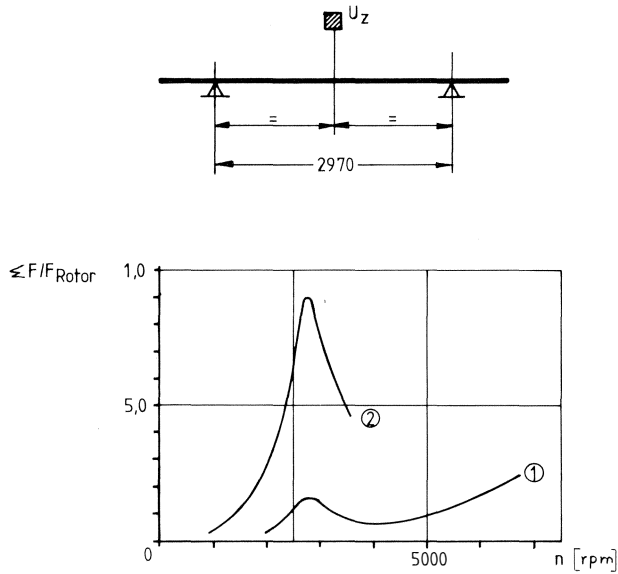
$\Sigma\,F\ =\ $ Sum of dynamic bearing forces at front and rear journal bearing

$F_{Rotor}\ =\ $ Rotor weight $= 30670$ N

$\dfrac{\Sigma\,F}{F_{Rotor}}\ =\ $ Relative dynamic bearing force of rotor

①   Balanced rotor as in Fig.2

②   Rotor as in 1 but with artificial unbalance U_Z at center of rotor. $U_Z\ =\ 60{\times}10^3$ mmg *)

     *) This unbalance corresponds at $n = n_{K1} = 2971$ rpm to balance grade $Q = 5.9$ mm/s.

Figure 13. Dynamic Bearing Force of the Rotor as in Figure 2 with Different Values of Unbalance.
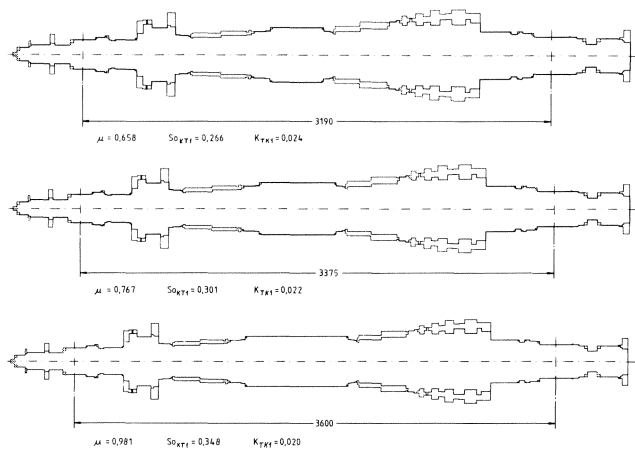
Figure 14. Variation in Shaft Elasticity by Enlarging the Bearing Span of the Rotor as in Figure 2.
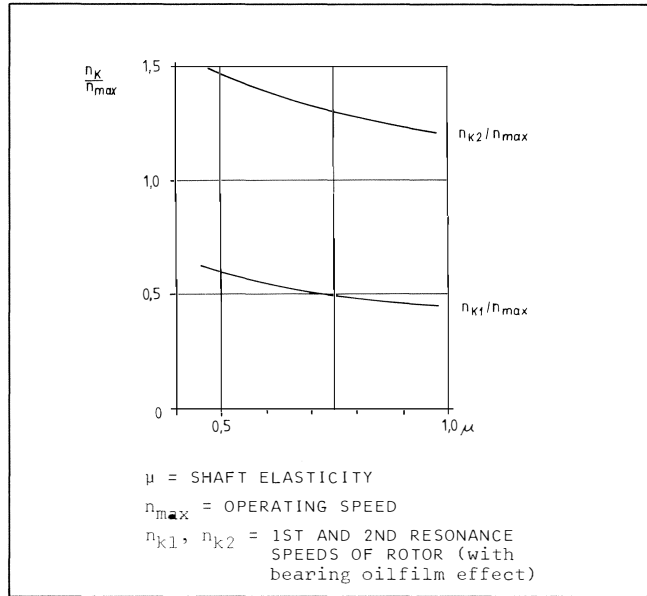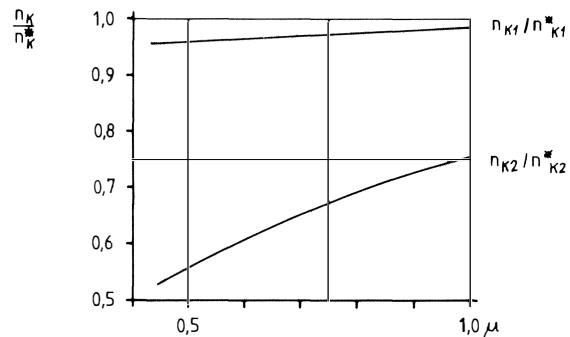
$\mu\ =\ $ SHAFT ELASTICITY

$n_{max}\ =\ $ OPERATING SPEED

$n_{K1}, n_{K2}\ =\ $ 1ST AND 2ND RESONANCE SPEEDS OF ROTOR (with bearing oilfilm effect)

Figure 15. 1st and 2nd Resonant Speeds as a Function of Shaft Elasticity.

$\mu\ =\ $ Shaft elasticity

$n_{K1}, n_{K2}\ =\ $ 1st and 2nd resonant speed of rotor - with bearing oil film in effect

$n_{K1}^*, n_{K2}^*\ =\ $ 1st and 2nd critical rotor speed - for rigid bearings

Figure 16. Resonant Speed/Critical Speed as a Function of Shaft Elasticity.

sonant speed. This aspect must be considered closely for disturbance conditions which can give rise to major center unbalances. The resulting resonant amplitude values could quite possibly represent a design limit for the shaft elasticity.

The resonant amplitude values were also calculated for four-wedge bearings in order to clarify the effect of the bearing shape on resonant amplitudes. The rotor geometry was unchanged. The four-wedge bearing has poorer damping properties than the two-wedge bearing because of its less sharply curved bearing shells, so even at $\mu = 0.5$ the resonant amplitude is considerably greater than that with a two-wedge
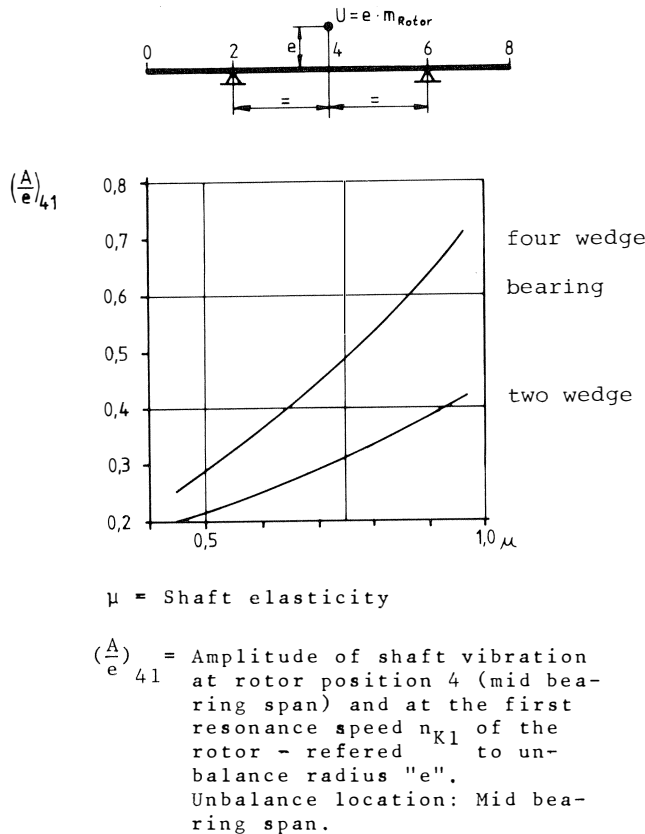
$(\frac{A}{e})_{41}$ = Amplitude of shaft vibration at rotor position 4 (mid bearing span) and at the first resonance speed n_{K1} of the rotor - refered to unbalance radius "e". Unbalance location: Mid bearing span.

Figure 17. Amplitude at Rotor Center for 1st Resonant Speed as a Function of Shaft Elasticity and Bearing Form.

bearing. With an increasing value of μ the discrepancy compared with the two-wedge bearing becomes steadily greater. Double the value for μ gives a three times greater resonant amplitude for the four-wedge bearing.

The two-wedge bearing is clearly superior to the four-wedge type with respect to the damping of unbalance vibrations.

However, for a bearing rotor system it is not only the behavior with forced unbalance vibration which has to be considered, but also its stability against self-excited vibration. Such self-excited vibration occurs above a certain limit speed. It is typified by large amplitudes and vibration frequencies which are considerably lower than the rotational frequencies.

This limit speed, called the stability limit, is much higher with four-wedge bearings than with two-wedge bearings, however (see Figure 18). Therefore, it is frequently necessary to strike a balance between the damping of unbalance vibration and the necessary stability reserve which the use of four-wedge bearings makes essential. Figure 18 illustrates the effect of shaft elasticity on the stability limit. With four-wedge bearings the limit speed clearly decreases with increasing shaft elasticity.

With two-wedge bearings the limit speed in the μ range being studied increases slightly with increasing elasticity and decreases again when higher μ values are reached. In general, the limit speed falls with increasing shaft elasticity.

Increasing shaft elasticity has two negative effects on the rotor dynamics: the resonant amplitude values of unbalance vibration increase, and the limit speed for the occurrence of self-excited vibration is reduced.
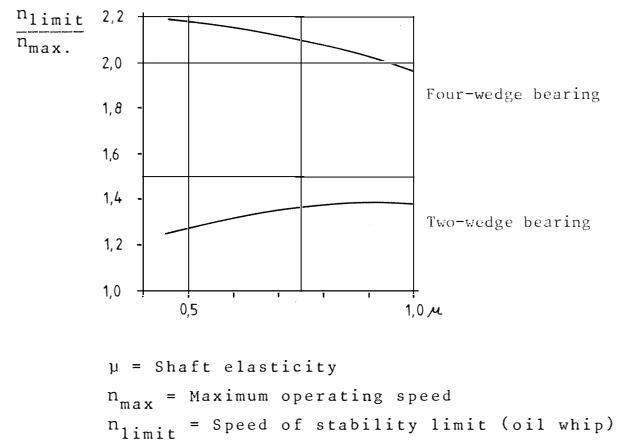

μ = Shaft elasticity

n_{max} = Maximum operating speed

n_{limit} = Speed of stability limit (oil whip)

Figure 18. Stability Limit as a Function of Shaft Elasticity and Bearing Form.

ROTOR FOR A CONDENSING TURBINE WITH COUPLING WEIGHTS AT BOTH SHAFT ENDS

The rotor studied so far had simply one coupling so only one of the two shaft ends was loaded with a large mass. In order to examine the effect on the resonant speeds, the resonant amplitude; and the dynamic bearing forces of a mass on the previously free shaft end; a mass of 70 kg was shrunk on to the free shaft end. This corresponded to the mass of the coupling on the original rotor.

Numerical computations and balancing measurements were then performed for the modified rotor.

Figure 19 shows the rotor fitted with the extra mass. Figure 20 shows the subdivision of the rotor into sections for calculation of the rotor dynamics.

In Figures 21, 22, and 23 the calculated relative values of rotor amplitude are plotted as a function of speed. These graphs are directly comparable with those in Figures 4, 5 and 6.

A comparison shows that the first resonant speed is changed but little in position and magnitude by the extra mass. The second resonant speed, on the other hand, is clearly much lower: it has fallen from $n_{k2} = 7154$ rev/min to $n_{k2} = 5868$

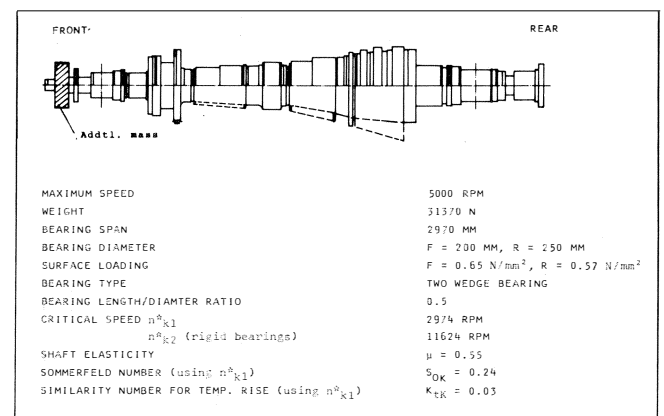|	
MAXIMUM SPEED	5000 RPM
WEIGHT	31370 N
BEARING SPAN	2970 MM
BEARING DIAMETER	F = 200 MM, R = 250 MM
SURFACE LOADING	F = 0.65 N/mm², R = 0.57 N/mm²
BEARING TYPE	TWO WEDGE BEARING
BEARING LENGTH/DIAMTER RATIO	0.5
CRITICAL SPEED n^*_{K1}	2974 RPM
n^*_{K2} (rigid bearings)	11624 RPM
SHAFT ELASTICITY	$\mu = 0.55$
SOMMERFELD NUMBER (using n^*_{K1})	$S_{OK} = 0.24$
SIMILARITY NUMBER FOR TEMP. RISE (using n^*_{K1})	$K_{tK} = 0.03$

Figure 19. Rotor of Condensing Turbine Under Study with Extra Mass at the Front; Principal Data.
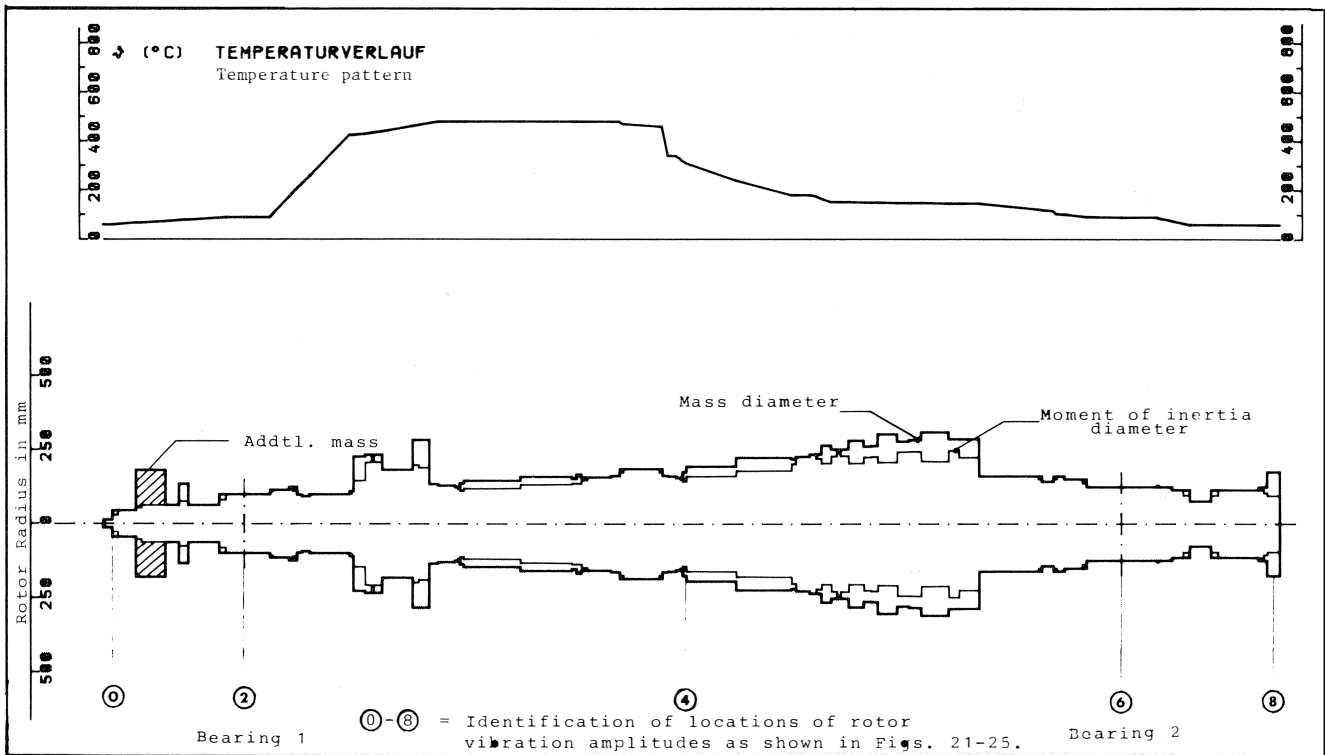
Figure 20. Subdivision of the Rotor with the Extra Front Mass Into Sections; Pattern of Rotor Temperature and Location of Points for the Calculation of Rotor Vibration Amplitudes.
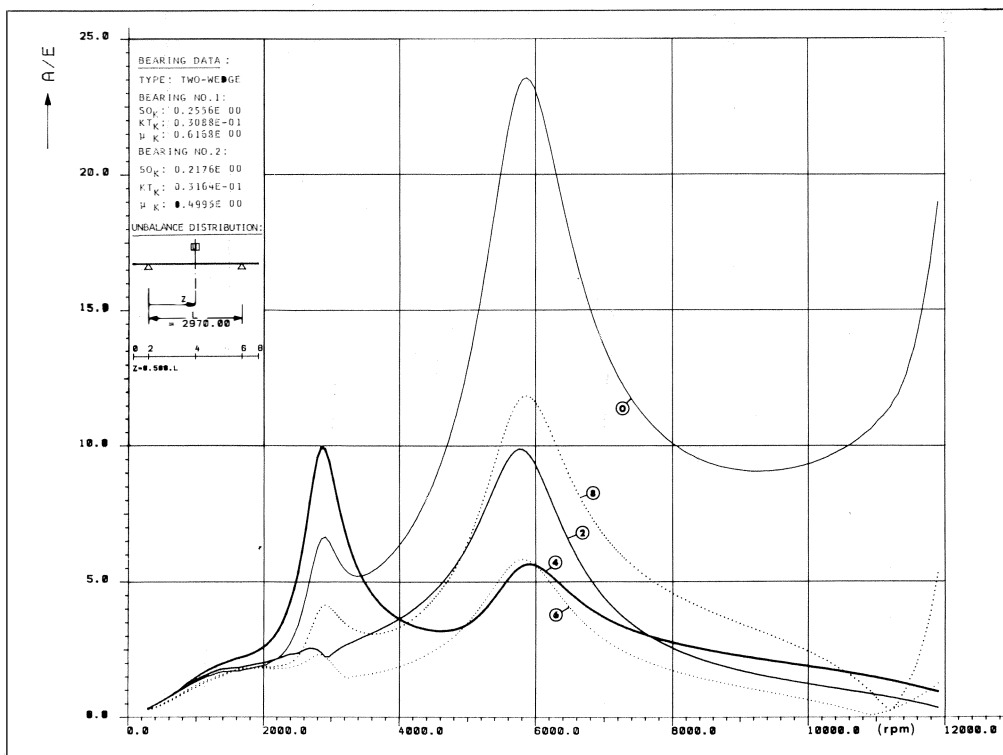

Figure 21. Relative Amplitude Values of Shaft Vibration as a Function of Speed for One Unbalance in the Center of the Rotor (Rotor as in Figure 19, Location of Calculation Points as per Figure 20).
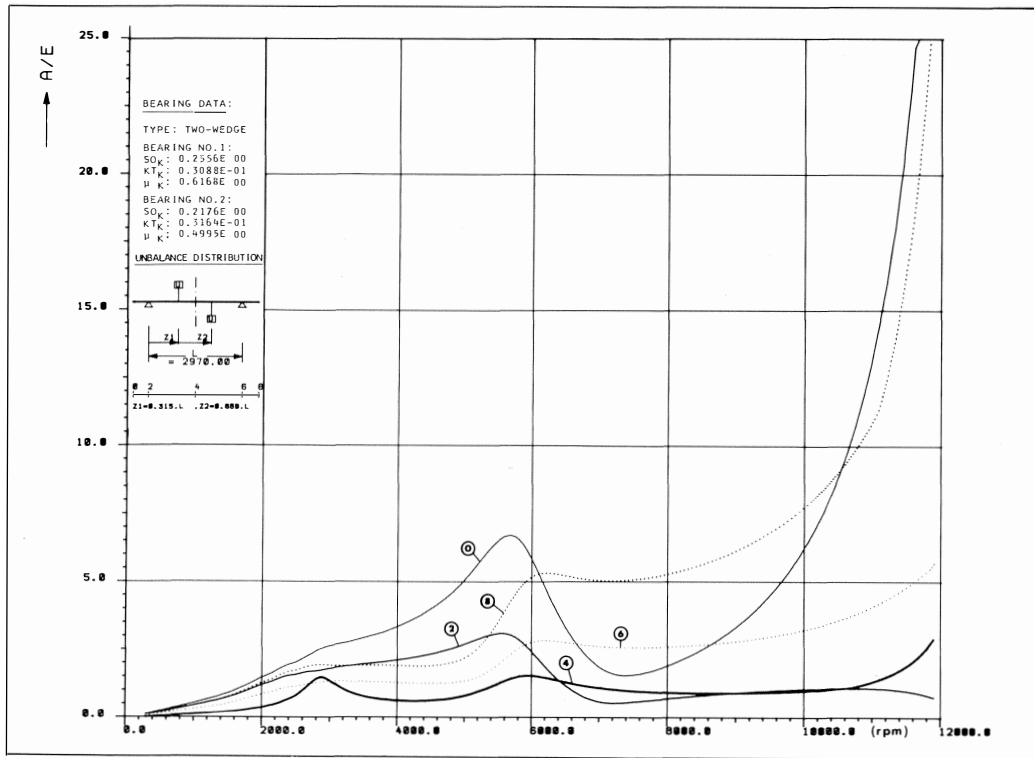
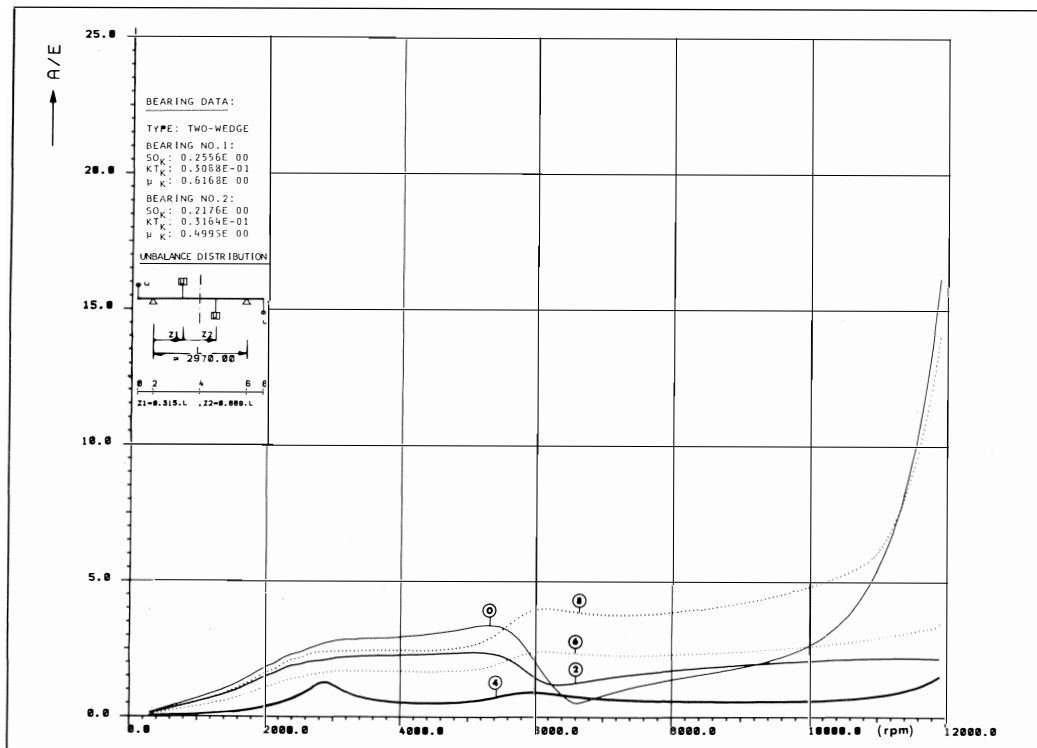*Figure 22. As Figure 21, but with Two Unbalance Points in Opposite Phase.*

Figure 23. As Figure 21, but with Four Unbalance Points in Opposite Phase.
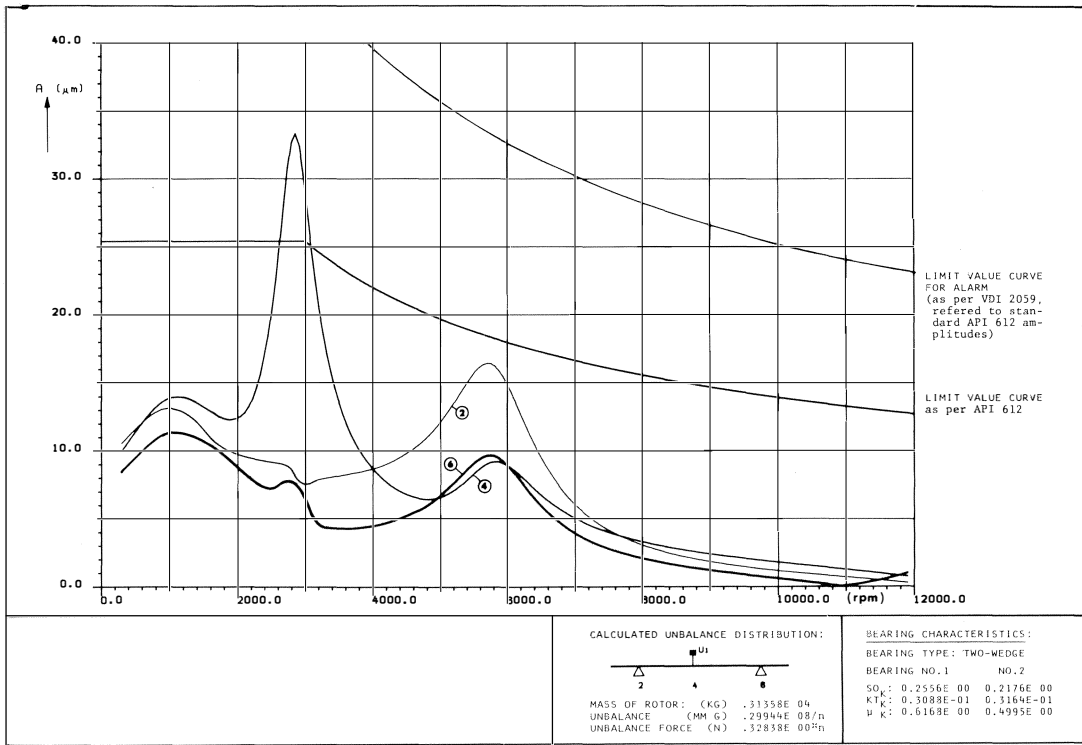
Figure 24. Amplitude Values of Shaft Vibration for Unbalance Corresponding to Balance Grade Q = 1 of the Rotor as in Figure 19, Location of Calculation Points as per Figure 20.
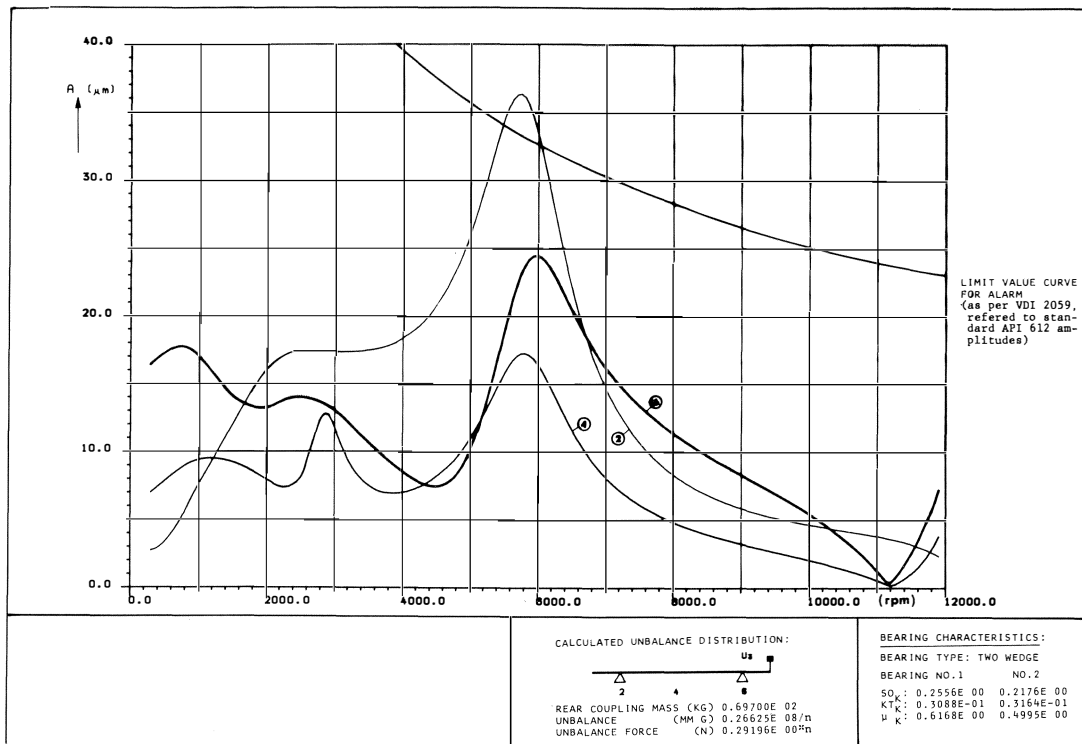

Figure 25. Amplitude Values of Shaft Vibration for a Coupling Unbalance Corresponding to Balance Grade Q = 40 of the Coupling (Rotor as in Figure 19, Location of Calculation Points as Per Figure 20).

rev/min. This results in the usable speed range between n_{k1} and n_{k2} being greatly curtailed.

The resonant amplitude, however, is increased only slightly. A comparison of the amplitude values of a rotor with a center unbalance corresponding to balance grade Q = 1 having a limit curve to API 612 shows the same picture for the rotor with the extra mass as without it (see Figures 7 and 24). The same applies to the amplitude values of the rotor with a coupling unbalance corresponding to balance grade Q = 40 (see Figures 8 and 25).

The magnitudes of the amplitude values have hardly changed, but the second resonant speed has fallen sharply. The curve of the second resonant point of the rotor with the extra mass is, however, steeper than that of the original rotor, which suggests lower damping coefficients.

The main effect of the extra mass on the free shaft end, therefore, is to displace the second point of resonance considerably towards lower speeds.

The μ value of the rotor is hardly changed by the fitting of the extra mass. The position and magnitude of the first resonance are also unchanged. This confirms the suitability of the μ value as a similarity number for the first resonance. But despite identical μ values, the two compared rotors have very different second resonant speeds. Therefore, the μ value is unsuitable as a similarity number for the second point of resonance. This is not surprising since μ was defined for a single-mass vibration system.

Everything which has already been said for Figures 9 to 12 is applicable to the deflection curves of the rotor with the extra mass (see Figures 26, 27, 28 and 29). The deflection curves are almost identical to those of the rotor without the extra mass. They have also been calculated for a center unbalance in Figures 26 to 28. The calculation speeds chosen were n = 1000 rev/min, n_{k1} = 2852 rev/min, n = 4500 rev/min and n_{k2} = 5868 rev/min.

Figure 30 shows the results of tests conducted on the rotor during balancing. As in Figure 13 the sum of the dynamic forces measured at both bearings are plotted as a function of speed. The sum of the forces is referred to the rotor weight. Curve 1 represents the variation in dynamic bearing forces as a function of speed for the properly balanced rotor.

Throughout the speed range the dynamic bearing forces are less than 10% of the rotor weight. Thus the rotor with two coupling masses can also be balanced well.

Curve 2 was measured after an artificial unbalance of only 0.72×10^3 mmg (corresponding to a mass of 4 grams) had been applied to the extra mass. At speed n_{k1} this unbalance corresponds to a balance grade of Q = 3 referred to the mass of the additional unbalance.

Even this small unbalance results in approximately three times greater dynamic bearing forces at the resonant speeds compared with the properly balanced rotor. This means that the "overhanging end" of the rotor is very sensitive to unbalance.

Curve 3 is the result of measurements taken with an artificial unbalance of 30×10^3 mmg applied to the middle of the properly balanced rotor with no artificial unbalance on the extra mass. At speed n_{k1} this unbalance corresponds approximately to balance grade Q = 3. Since only the behavior of the rotor when passing through the first resonant speed was to be examined, the measurements were only taken for speeds below 3000 rev/min.

The sum of the dynamic bearing forces at n_{k1} attains approximately 55% of the shaft weight.
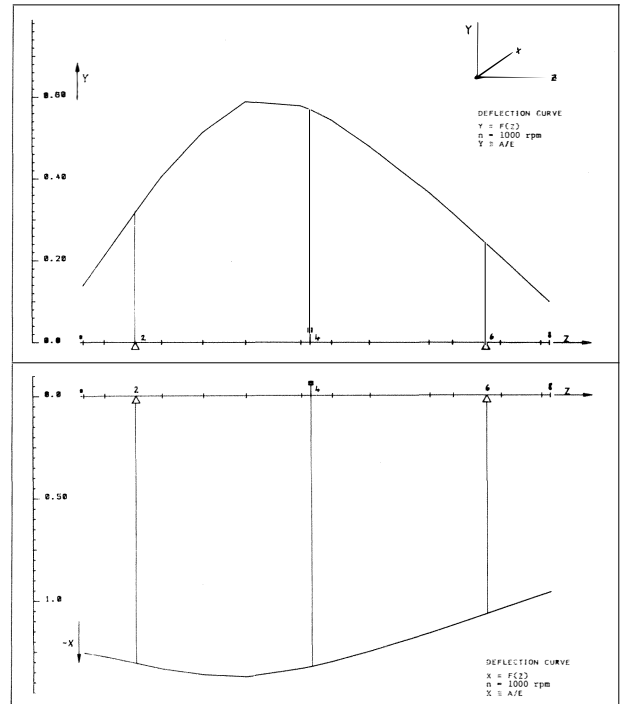

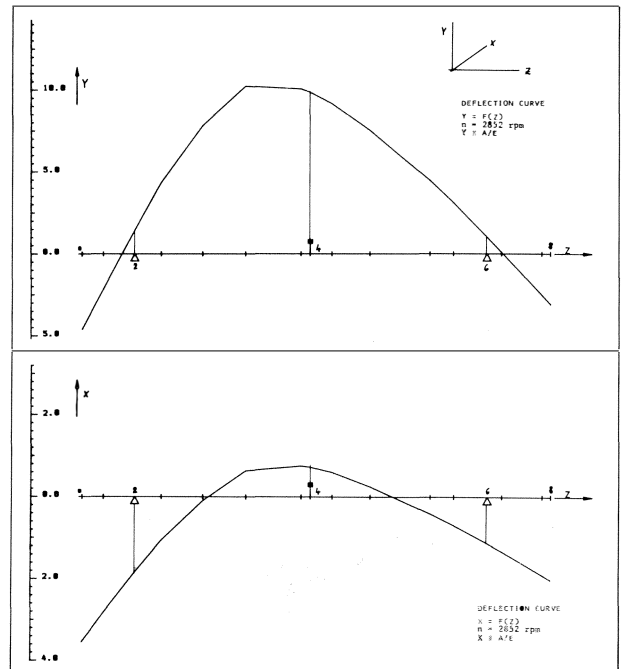Figure 26. Deflection Curve for Unbalance at the Middle of the Rotor, n = 1000 rev/min (Rotor as in Figure 19).

Figure 27. As Figure 26, but n = 2853 rev/min.

Curve 4 was obtained under the same conditions as curve 3, except that the unbalance was doubled to 60×10^3 mmg. The dynamic bearing force at the first resonant speed is increased to approximately 95% of the rotor weight. This value is almost identical to that of the rotor without the extra mass
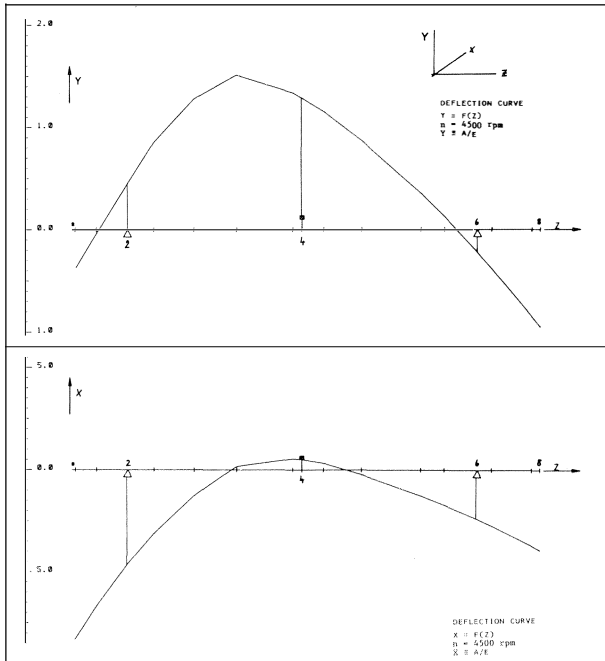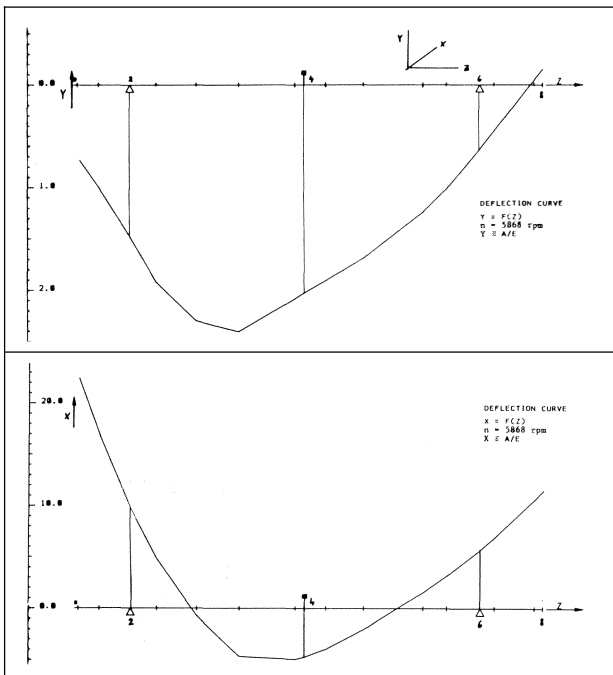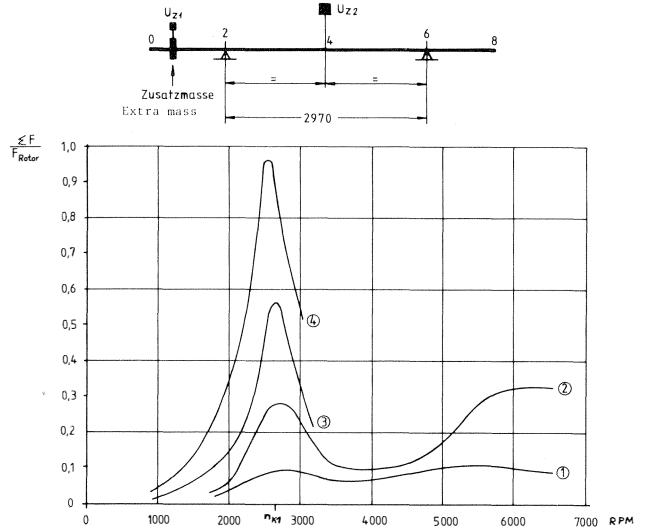
Figure 28. As Figure 26, but n = 4500 rev/min.

Figure 29. As Figure 26, but n = 5868 rev/min.

ΣF = SUM OF DYNAMIC BEARING FORCES AT FRONT AND REAR JOURNAL BEARINGS.

F_{Rotor} = 31370 N (ROTOR WEIGHT)

$\dfrac{\Sigma F}{F_{Rotor}}$ = RELATIVE DYNAMIC BEARING FORCE OF ROTOR

① BALANCED ROTOR AS IN FIG.19: $U_{Z1}=0$, $U_{Z2}=0$

② ROTOR AS ABOVE, BUT WITH ARTIFICIAL UNBALANCE U_{Z1} APPLIED TO THE EXTRA MASS. $U_{Z1}= 0.72X10^3 mmg$ *)
$U_{Z2}= 0$

*) This corresponds to a balance grade Q=3.1 when refered to the unbalance mass, and to Q=0.07 when refered to the total rotor mass, at n_{K1}

③ ROTOR AS ABOVE, BUT WITH ARTIFICIAL UNBALANCE U_{Z2} APPLIED TO THE ROTOR CENTER. $U_{Z1}= 0$
$U_{Z2}= 30X10^3 mmg$ *)

*) This corresponds to a balance grade Q=2.9 when refered to the total rotor mass at n_{K1}

④ ROTOR AS IN 3 ABOVE, BUT MASS OF ARTIFICIAL UNBALANCE IN ROTOR CENTER DOUBLED TO $U_{Z2}= 60X10^3 mmg$ *). $U_{Z1}=0$

*) This mass now corresponds to balance grade Q=5.8, at n_{K1} and refered to the total rotor mass.

Figure 30. Dynamic Bearing Force of the Rotor as in Figure 19 for Various Values of Unbalance.

up to dynamic bearing forces of the order of magnitude of the rotor weight.

The tests have shown that extra masses on the ends of the rotor have very little effect on the first resonant point of the rotor. Such extra masses, however, have a serious effect on the position of the second point of resonance. The effect of unbalance at the middle of the rotor is largely unchanged by the extra mass. Unbalance in the masses at the free ends of the rotor, on the other hand, has a serious effect on the rotor dynamics.

REFERENCES

1. Glienecke, J.: "Feder- und Dämpfungskonstanten von Gleitlagern für Turbomaschinen und deren Einfluss auf das Schwingungsverhalten eines einfachen Rotors." Thesis, Techn. Hochschule Karlsruhe, 1966.

2. Pollmann, E.: "Berücksichtigung der veränderlichen Öl-viskosität bei der Berechnung von Gleitlagern." *Konstruktion* 19(1967) Vol. 5.

(Figure 13). The point of resonance could be passed through without difficulty.

For the properly balanced rotor, the dynamic bearing force at n_{k1} was approximately 10% of the rotor weight. The increase in dynamic bearing force resulting from the center unbalances was therefore 45% and 85%. With good accuracy, therefore, it means that doubling the unbalance doubles the dynamic bearing force. This linear relationship is at least valid

3. Pollmann, E.: "Das Mehrgleitflächenlager unter Berücksichtigung der veränderlichen Ölviskosität." *Konstruktion* 21 (1969) Vol. 3, pp. 85 to 97.

4. Glienecke, J.: "Experimentelle Ermittlung der statischen und dynamischen Eigenschaften von Gleitlagern für schnellaufende Wellen - Einfluss der Schmierspaltgeometrie und der Lagerbreite." *Fortschrittsberichte der VDI-Zeitschriften,* Series 1, No. 22, 1970.

5. Glienecke, J.; Dabrowski, K.: "Berechnung der Unwuchtschwingunge eines allgemein gleitgelagerten Läufers." *Forschungsvereinigung Verbrennungskraftmaschinen e.V.,* Vol. 118 (1971).

6. Wolter, I.: "Research on Rotor Dynamics in Industrial Turbines," *Siemens Review* XL(1973), pp. 566 to 574.

7. Glienecke, J.: "Einfluss der Lagerparameter und der Wellensteifigkeit auf das Schwingungsverhalten einer Rotors." *MTZ (Motortechnische Zeitschrift),* 32, No. 4/1971.

8. APT-Norm 612: "Spezial-Dampfturbinen für Raffineriebetrieb." American Petroleum Institute.

9. VDI-Richlinie 2060: "Beurteilungsmassstäbe für den Auswuchtzustand rotierender starrer Körper." Verein Deutscher Ingenieure.

10. VDI-Richtlinie 2059, Blatt 3 (Entwurf VDI/W-16): "Wellenschwingungen von Industrieturbosätzen, Messung und Beurteilung." Verein Deutscher Ingenieure.